Crystallization Signatures as Predictive Biomarkers in Histopathology

C. Dumitrescu, D. Hackel, I. Obeid and J. Picone

Neural Engineering Data Consortium, Temple University, Philadelphia, Pennsylvania, USA
{claudia-anca.dumitrescu, dmitry.hackel, iobeid, picone}@temple.edu

***Abstract*— Crystallization processes in soft tissues have long been studied in relation to pathology and have been shown to positively correlate with precursory pathological cell activity. Early detection of breast cancer remains a daunting challenge in artificial intelligence, partly due to the prevalence of overdiagnosis and a lack of transparency in experimental results. Among histopathological specimens, tissue calcifications, ranging from dystrophic hydroxyapatite deposits to idiopathic oxalate crystals and psammoma bodies, have long held diagnostic promise but remain underexploited by visual models.**

In this paper, we introduce a novel crystallization-focused approach to multi-classification tasks derived from the Fox Chase Cancer Center Breast Tissue Corpus (FCBR). We constructed an annotated subset comprising 439 patches categorized into Crystalline Non-Neoplastic (cnno: n = 51), Crystalline Ductal Carcinoma in Situ (cdcs: n = 168), and Crystalline Invasive Ductal Carcinoma (cidc: n = 220).

Leveraging this subset, we conducted a baseline experiment comparing a simple Random Forest classifier trained on (1) a standard, non-crystallization dataset (1,850 patches) versus (2) an enriched dataset including the crystallization annotations (2,243 patches). Models were evaluated on held-out FCBR samples (18,224 patches) and externally validated on the Temple University Hospital Digital Pathology (TUDP) Corpus (46,666 patches). Incorporation of crystallization annotations more than doubled the overall accuracy: from 18.4% to 34.6% on FCBR and from 20.7% to 23.5% on TUBR. These improvements persisted under domain shift, indicating enhanced generalization and statistical significance.

Our findings demonstrate that explicit modeling of microcalcification patterns provides biologically meaningful features that strengthen deep learning based breast cancer detection. We propose that further expansion of crystallization annotations, especially for underrepresented non-neoplastic cases, and integration into more complex architectures may drive additional gains in sensitivity and diagnostic granularity.

Keywords*— *breast cancer, calcification, histopathology, microcalcification, crystallization, biomarkers

I. Introduction

Crystallization in tissue refers to the formation and deposition of microscopic crystals within biological tissue [1]. Healthy tissues, such as bone and teeth, naturally regulate these processes. Recent studies [2] highlighted that ectopic calcification is often an active, cell-driven process, contrary to the expectation of passive precipitation, and that intracellular Ca^{2+} signaling is central to both physiological mineralization and pathological calcification. This shifts the view of calcification from being solely a product of aging or genetics to a potentially preventable process, monitorable, and treatable. A detailed understanding of its underlying mechanisms is therefore essential for clarifying its role in pathophysiology.

In breast cancer, calcifications arise through active processes promoted by the presence of cancer that mirror aspects of human physiology [3]. Some examples are shown in Figure 1. Cancer cells and adjacent stromal tissue can undergo osteogenic-like reprogramming, characterized by upregulation of transcription factors such as Runx2 and Osterix. This promotes the deposition of calcium phosphate, predominantly hydroxyapatite ($Ca_{10}(PO_4)_6(OH)_2$) and calcium oxalate (CaC_2O_4), which serve as the components of calcification.

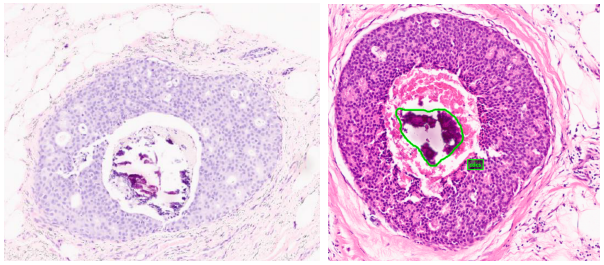

(a) samples of calcification associated with DCIS

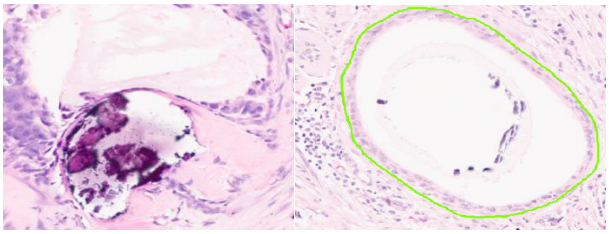

(b) samples of calcification associated with NNEO

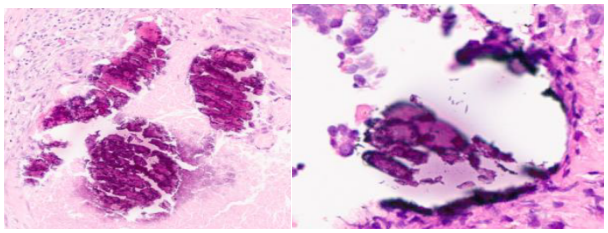

(c) samples of calcification associated with INDC

Figure 1. Examples of calcification in a breast tissue image

Necrosis, apoptotic bodies, and matrix vesicles released by tumor cells generate localized niches enriched with calcium and phosphate-binding proteins, while showing reduced concentrations of calcification inhibitors such as matrix Gla protein and fetuin-A. This breast cancer–derived microenvironment fosters hydroxyapatite and calcium oxalate crystal growth, rendering calcification a defining non-neoplastic hallmark breast cancer. Nevertheless, mechanistic understanding remains incomplete [2], unexplored in computer vision.

Early detection of cancer remains a profound challenge in modern oncology [4]. The meta-analysis [5] reported mean sensitivity of 96.3% (CI 94.1–97.7) and specificity of 93.3% (CI 90.5–95.4), respectively, yet found that 99% of included studies had at least one area of high or unclear risk of bias, underscoring persistent limitations in the current state of the art. Routine yearly imaging in asymptomatic people does not reduce mortality compared to regular check-ups and often reveals noncancerous lesions. For instance, about 22% of breast cancer cases are overdiagnosed [4]. One of the most dependable clues doctors look for in breast tissue is calcifications, long recognized as an important diagnostic marker. However, their full potential remains underexplored in the era of modern artificial intelligence (AI). In this study, we leverage mineral deposit signatures as morphological biomarkers to investigate the role of tissue crystallization in cancer detection.

II. Pathological Crystallization

Pathological crystallization [6] in human tissues encompasses a variety of processes by which calcium salts and, in some cases, ionic structures are deposited in soft tissues under pathological conditions, such as chronic inflammation [7]. Some examples are shown in Figure 1. Soft-tissue mineralization segregates into two primary crystal classes: Type I (calcium oxalate) and Type II (calcium phosphate/hydroxyapatite).

Recent investigations [8] have increasingly suggested that specific mineral compounds may be linked to the development and progression of cancer. In breast lesions such as ductal carcinoma in situ (dcis) studies report that hydroxyapatite deposits are more frequent than in benign tissue. These deposits show reduced carbonate substitution and elevated magnesium-whitlockite, features that correlate with lesion grade and biological aggressiveness. Shin et al. [3] reported findings that contradicted earlier associations of whitlockite with malignancy, and other studies [8] have more often connected this mineral with non-malignant processes. X-ray diffraction demonstrates potential clinical application, with measurements of carbonate substitution achieving a sensitivity of 85% and specificity of 88% in distinguishing benign and neoplastic cases using the average carbonate content alone [2].

In mammography, dystrophic calcification is the most common form and is independent of systemic calcium. Loss of membrane integrity allows intracellular calcium to flood into the extracellular space and precipitate with phosphate, forming hydroxyapatite crystals in mitochondria and the surrounding matrix [9]. In contrast, metastatic calcification results from elevated serum calcium or phosphate, often due to hyperparathyroidism or chronic renal failure, leading to diffuse crystal deposition in otherwise healthy tissues. While metastatic calcifications typically affect the kidneys, lungs, and gastric mucosa, rare cases of breast parenchymal involvement have been reported in long-term hemodialysis patients and those with secondary hyperparathyroidism [10].

Secretory calcification, or idiopathic crystal deposition within glandular lumina, results in calcium oxalate (weddellite) crystals (type I calcifications) most often in apocrine cysts of the breast. These birefringent, concentric crystals form within secretions and are typically benign. Their presence can occasionally coincide with proliferative lesions such as lobular carcinoma in situ [6].

Certain neoplasms generate psammoma bodies, concentric, lamellated calcium spherules thought to arise via dystrophic mechanisms within papillary tumor structures. In invasive micropapillary carcinoma of the breast, psammoma bodies have been observed in up to 64% of cases, reflecting localized cell death and mineral nucleation within micropapillary clusters [11].

Tumoral calcinosis and calcinosis cutis represent massive calcium phosphate accumulation, but the frequency is relatively low, especially in breast tissue. Another example of such rare formations is heterotopic ossification, representing true lamellar bone formation, with organized cortical and trabecular architecture, within soft tissues following trauma, surgery, or neurologic injury. This process, in which mesenchymal cells differentiate into osteoblasts outside the skeleton, occur in muscle and periarticular tissues and is distinct from amorphous calcific deposits [12].

In this paper, we focus on, as shown in Table 1, the distinctive calcification patterns in breast tissue, exploring how these diverse pathological crystalline deposits can be quantitatively characterized and integrated into AI-driven models for improved cancer detection of 9 classes. For additional details on each pathological structure or resolution and magnification, please refer to [12]. We hypothesize that calcifications may serve as discriminative morphological markers, offering an opportunity for deep learning models to enhance the diagnosis and efficiency of cancer detection by leveraging clinical reasoning.

Table 1. Labels used for annotation of TUBR and FCBR

Label	Description / Features
Normal (norm)	normal ducts and lobules
Ductal Carcinoma in Situ (dcis)	ductal carcinoma in situ, and lobular carcinoma in situ
Invasive Ductal Carcinoma (INDC)	invasive ductal carcinoma, invasive lobular carcinoma, and invasive mammary carcinoma
Non-Neoplastic (NNEO)	fibrosis, hyperplasia, intraductal papilloma, adenosis, ectasia, etc.
Inflammation (INFL)	areas of inflammation
Artifact (ARTF)	grease pen marks, stitches, foreign bodies, etc.
Indistinguishable (NULL)	indistinguishable tissue, normally due to issues with the cut/stain
Suspected (SUSP)	regions that are at risk of developing into cancerous regions
Background (BCKG)	stroma, no ducts or lobules

III. FCCC Breast Crystallization subset

The Neural Engineering Data Consortium (NEDC) has released two significant open-source annotated digital pathology datasets related to breast tissue [13]: the Temple University Hospital Digital Pathology Corpus Breast Tissue Subset (TUBR) and the Fox Chase Cancer Center (FCCC) Digital Pathology Corpus Breast Tissue Subset (FCBR). A summary of the labels used in these corpora is given in Table 1. The process of annotating these corpora is described in detail in [13] and serves as a basis for this work.

Since FCCC specializes in cancer treatment, the FCBR data represent a large sample of the most common and most dangerous types of breast cancer – invasive ductal carcinoma. The FCBR contains 12,164 non-cancerous, 1,967 carcinogenic, and 5,954 cancerous identified structures. This corpus, heavily weighted towards malignant pathology, was selected as the basis for constructing a new subset focused specifically on tissue crystallization phenomena. To our knowledge, no other open-source subset exists that isolates and annotates crystallization patterns in breast histopathology.

Crystallization profiles differ depending on the pathological structure with which they are associated. For example, crystalline non-neoplastic (CNNO) structures tend to present with discrete, loosely clustered calcific fragments typically isolated within fibroglandular stroma. Crystalline ductal carcinoma in situ (CDCS) structures display larger, denser, and more irregular mineral formations situated within atypical ductal epithelial arrangements. In crystalline invasive ductal carcinoma (CIDC) cases, the calcifications are often embedded within chaotic, infiltrative patterns consistent with stromal invasion. These findings highlight microstructural markers that may help distinguish borderline or ambiguous lesions.

Annotations were produced by manually outlining the complete region of interest with contours drawn as tightly as possible around its boundaries. The annotations were then cross-validated by an annotation team that had been responsible for annotation of TUBR and FCBR. To facilitate structured analysis, we organized the crystallization annotations into three distinct classes, based on visual and spatial characteristics of the calcific deposits: CNNO (n = 51), CDCS (n = 168), CIDC (n = 220). This categorization was informed by observed variations in morphology, localization and spatial distribution of the calcific material. Each category has distinct diagnostic implications.

Through our manual annotation process, we identified 117 images files from 116 unique subjects in the augmented the original FCCC dataset. These images contain a total of 439 annotated patches. We will refer to these 439 images as the Fox Chase Crystallization Corpus (FCCR). Due to the limited number of instances of crystallization in FCBR, we added all these images to the training data for FCBR, creating some overlap in the subject population with the evaluation set.

To partition this new hybrid corpus (FCBR+FCCR) into /train, /dev and /eval, we followed the protocol described in [15] for TUBR, in which a wide variety of demographic and morphological features (e.g., malignancy grade) were balanced across the three subsets. Out of 687 subjects in the original FCBR evaluation data, there are 52 subjects that are common to the training and evaluation data in this new hybrid corpus. However, no images are duplicated between these three segments of the corpus. Further, there is no overlap between TUBR and FCCR since the FCCR annotated data was selected only from FCBR.

IV. Experimental Results

To evaluate the discriminative power of calcification patterns in histopathological classification, we conducted a baseline experiment to determine whether the inclusion of crystalline annotations improved predictive accuracy. The results of these experiments are summarized in Table 2 through Table 5.

An overview of the experimental workflow is shown in Figure 2. All experiments were run with a fixed random seed (42) to ensure reproducibility. For this proof-of-

Table 2. Confusion matrix and accuracy for FCBR

Fox Chase Cancer Center Breast Tissue Subset (FCBR)		
Metric	**Crystal**	**Non-Crystal**
Correct	6,308	3,345
Incorrect	11,916	14,879
Accuracy	34.6%	18.4%

Table 3. Comparison of the suspicious classes for FCBR

Fox Chase Cancer Center Breast Tissue Subset (FCBR)		
Class	**Accuracy (Crystal)**	**Accuracy (Non-Crystal)**
INDC	19.1%	5.0%
DCIS	17.2%	8.5%
NNEO	7.5%	2.7%

Table 4. Confusion matrix and accuracy for TUBR

Temple University Digital Pathology Breast Tissue Subset (TUBR)		
Metric	**Crystal**	**Non-Crystal**
Correct	10,968	9,681
Incorrect	35,698	36,985
Accuracy	23.5%	20.7%

Table 5. Comparison of the suspicious classes for the TUBR

Temple University Digital Pathology Breast Tissue Subset (TUBR)		
Class	**Accuracy (Crystal)**	**Accuracy (Non-Crystal)**
INDC	17.95%	4.97%
DCIS	20.68%	6.10%
NNEO	4.40%	2.72%

concept baseline, annotated images were converted to binary (black-and-white) masks, resized to 256x256 pixels, flattened into 65,536-dimensional vectors, and used as input to a Random Forest (RNF) model available in the MIT-licensed library imbalanced-learn (v0.14.0) [14]. This simple preprocessing and model choice was intentional, yielding a transparent, computationally inexpensive robust baseline.

This choice requires minimal hyperparameter tuning and facilitates direct comparison with future, complex architectures. Imbalanced-learn was used to address class imbalance during training. We acknowledge that flattening removes spatial information from the images. More advanced methods that preserve spatial structure (patch-based CNNs or engineered texture features) are recommended for follow-up work.

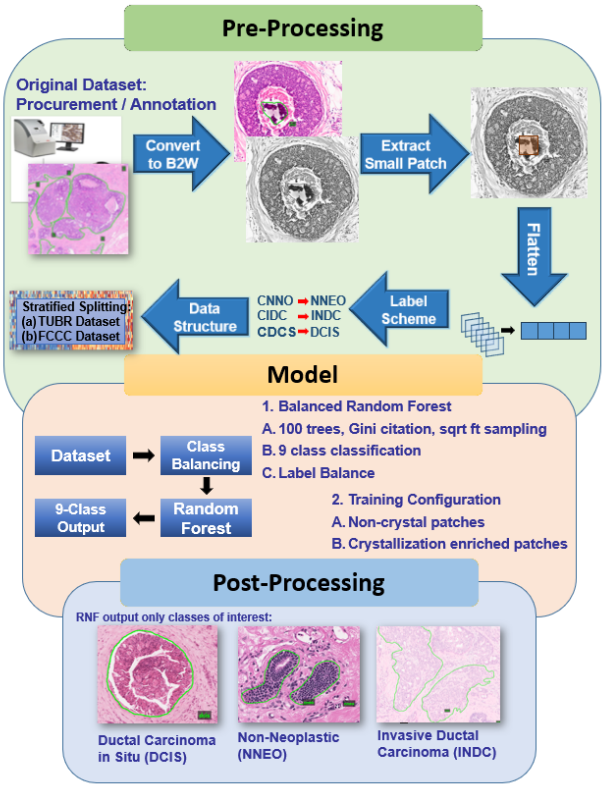

Figure 2. The crystallization baseline experiment workflow

This balanced RNF model was trained on two separate configurations: (1) a non-crystallization dataset consisting of 1,850 patches, and (2) a crystallization-enriched dataset containing 2,243 patches (FCBR+FCCR). The models were evaluated on the remaining portion of FCBR (comprising 18,224 patches) and further validated on TUBR (comprising 46,666 patches). The latter constitutes true open set testing since no TUBR data was annotated.

The balanced RNF algorithm handles imbalance at the sampling stage: for each tree, it draws a sample from the minority class (bootstrap) and samples an equal-sized set from the majority class (sampling with replacement) so every tree is trained on a balanced subset. For this baseline, we used the default hyperparameters: number of trees = 100, Gini split metric, sqrt features tried per split, unlimited depth, minimum split and leaf controls of 2 and 1, respectively. The sampling strategy was chosen to equalize all classes.

We used an RNF model because of its simplicity, speed, and stability. We have calibrated the performance of several deep learning models on this data in [13]. Performance is generally consistent – improvements with one classifier tend to hold up across other classifiers.

The inclusion of crystallization annotations improved the overall classification accuracy by more than doubling the

no-crystallization performance. In Table 2, we demonstrate significant gains in categories directly associated with calcification. These three classes are challenging to classify using standard approaches and significantly contribute to the overall error rate. The most notable improvement was observed in the INDC and DCIS classes, indicating that the additional annotations enabled the model to better distinguish between early-stage and invasive carcinoma phenotypes.

On the FCBR dataset, the crystallization model produced substantially improved per-class retrieval for the labels of interest: NNEO (Precision = 0.12, Recall = 0.076, F1 = 0.09), DCIS (Precision = 0.08, Recall = 0.18, F1 = 0.11), and INDC (Precision = 0.78, Recall = 0.23, F1 = 0.35). By contrast, the non-crystallization model on the same set yielded materially lower performance: NNEO (Precision = 0.05, Recall = 0.03, F1 = 0.03), DCIS (Precision = 0.08, Recall = 0.09, F1 = 0.08), and INDC (Precision = 0.78, Recall = 0.05, F1 = 0.09). These results show that annotation of crystallization primarily increased recall for DCIS and INDC while also improving F1 for all three target classes. Moreover, it doubled the overall accuracy (Δ = 16.26%). The 95% confidence interval for this accuracy difference is [15.37%, 17.15%], and the improvement was statistically significant ($p < 0.01$, McNemar's test). The largest gains occurred in INDC (Δ = 14.1%) and DCIS (Δ = 8.7%), which may possibly have been caused by the underrepresentation of the CNNO patches.

On the larger TUBR set the crystallization model's per-class metrics were lower in absolute terms but retained the same directional improvements: NNEO (Precision = 0.45, Recall = 0.04, F1 = 0.08), DCIS (Precision = 0.06, Recall = 0.21, F1 = 0.10), and INDC (Precision = 0.06, Recall = 0.18, F1 = 0.09). Under the non-crystallization condition, the corresponding values were: NNEO (Precision = 0.38, Recall = 0.03, F1 = 0.05), DCIS (Precision = 0.03, Recall = 0.06, F1 = 0.04), and INDC (Precision = 0.07, Recall = 0.05, F1 = 0.06). The crystallization model again outperformed the baseline (Δ = 2.76%, 95% CI = [2.23%, 3.29%], $p < 0.05$). Class-specific improvements were most pronounced for DCIS (Δ = 14.58%) and INDC (Δ = 13.00%), confirming that calcification annotations generalize beyond the original FCCC domain despite greater morphological variability.

In Table 3, we show the improvement in accuracy for each class. We see an across-the-board improvement in our ability to detect each of the three classes of interest. Each class experienced roughly a three-fold or greater improvement in absolute detection performance.

The gain in accuracy is less pronounced for TUBR. This is not surprising since TUBR contains a much wider range of morphologies. The overall accuracy in Table 4 increased by 20% and the per-class accuracies, as shown in Table 5, increased significantly. While the domain-shift results show a modest overall accuracy gain (from 20.7% to 23.5%, Δ = 2.8%, 95% CI = [2.23%, 3.29%], $p < 0.001$), this improvement, though statistically significant, may not yet be clinically transformative.

However, substantial per-class gains for DCIS (+14.58%) and INDC (+12.97%) suggest that calcification annotations enhance the detection of lesions with high diagnostic relevance. These results likely reflect greater morphological variability and staining differences in TUDP, emphasizing the need for domain adaptation and fine-tuning before deployment. Nonetheless, the observed improvements point toward the potential of crystallization modeling to strengthen diagnostic sensitivity in malignant categories, provided further validation and calibration are undertaken.

Results for both experiments demonstrate that the crystallization model exhibits better calibrated behavior, with fewer high-magnitude misclassifications across dominant classes like INDC and DCIS. In contrast, the non-crystallization model shows heavy confusion between malignant and background classes, likely due to missing structural cues associated with mineralization.

V. Summary

Our results suggest that the inclusion of annotated crystalline structures enhances a model's ability to detect biologically significant pathology, particularly across classes that exhibit microcalcification as a morphological hallmark. In malignant conditions (DCIS and INDC), the localization, density, and pattern of calcification can serve as distinct morphological signatures that complement cellular and stromal features. Our findings support the hypothesis that explicitly modeling these patterns enables a more nuanced understanding of breast cancer pathology and strengthens the diagnostic of deep learning models. By capturing subtle calcific patterns linked to tumor biology, crystallization provides a biologically meaningful feature set that enhances both sensitivity and generalizability across datasets.

The improvement in INDC performance may be explained by the heterogeneous and often infiltrative distribution of calcifications in invasive cancers, which, when annotated, offer additional spatial cues to the model. Similarly, in pre-invasive lesions like DCIS or NNEO, smaller or more localized calcifications serve as early morphological warning markers. These types of features are often underrepresented in models trained on general-purpose datasets with coarse labels. Expanding the CNNO annotation set may further improve performance on the NNEO class, which remains comparatively underrepresented, due to its higher prevalence in the TUBR dataset.

These findings suggest that integration of clinical reasoning into the model design, by incorporating calcification morphology and clinical context, moves towards a model that "thinks" like a pathologist . Clinically informed models allow for improved understanding of model predictions, providing a greater level of. Models that can distinguish between biologically meaningful calcifications and benign findings can aid in the reduction of overdiagnosis. Improved model performance can improve pathology workflows and prioritize high-risk slides for review. The results of our framework represent a step towards a clinically actionable, transparent, and generalizable breast cancer diagnostics model that aligns with the goals of precision medicine.

The curated crystal subset, FCCR, provides a resource for future computational pathology studies, exploring mineralization patterns as predictive or descriptive features of malignancy. The data is publicly available from our consortium website (*www.necdata.org*).

ACKNOWLEDGMENTS

This material is based on work supported by several organizations over the years including the National Science Foundation (grants nos. 1925494 and 1726188), the Temple University Catalytic Collaborative Funding Initiative and most recently by the Pennsylvania Breast Cancer Coalition Breast and Cervical Cancer Research Initiative. Any opinions, findings, and conclusions or recommendations expressed in this material are those of the author(s) and do not necessarily reflect the views of these organizations.

REFERENCES

[1] D. Proudfoot, "Calcium Signaling and Tissue Calcification," *Cold Spring Harbor perspectives in biology*, vol. 11, no. 10, Oct. 2019, doi: *10.1101/cshperspect.a035303*.

[2] A. Ali, Y. W. Chiang, and R. M. Santos, "X-ray Diffraction Techniques for Mineral Characterization: A Review for Engineers of the Fundamentals, Applications, and Research Directions," *Minerals*, vol. 12, no. 2, 2022. doi: *10.3390/min12020205*.

[3] K. S. Shin, M. Laohajaratsang, S. Men, B. Figueroa, S. M. Dintzis, and D. Fu, "Quantitative chemical imaging of breast calcifications in association with neoplastic processes," *Theranostics*, vol. 10, pp. 5865–5878, 2020. doi: *10.7150/thno.43325*.

[4] A. B. Miller, C. Wall, C. J. Baines, P. Sun, T. To, and S. A. Narod, "Twenty five year follow-up for breast cancer incidence and mortality of the Canadian National Breast Screening Study: randomised screening trial," *BMJ*, vol. 348, p. 10, 2014, doi: *10.1136/bmj.g366*.

[5] C. McGenity *et al.*, "Artificial intelligence in digital pathology: a systematic review and meta-analysis of diagnostic test accuracy," *npj Digit. Med.*, vol. 7, no. 1, Art. no. 1, May 2024, doi: 10.1038/s41746-024-01106-8

[6] J. E. Gonzalez, R. G. Caldwell, and J. Valaitis, "Calcium oxalate crystals in the breast. Pathology and significance," *Am J Surg Pathol*, vol. 15, no. 6, pp. 586–591, June 1991, doi: 10.1097/00000478-199106000-00007.

[7] F. Boraldi, F. D. Lofaro, and D. Quaglino, "Apoptosis in the Extraosseous Calcification Process," *Cells*, vol. 10, no. 1, p. 29, 2021. doi: *10.3390/cells10010131.*

[8] C. Morasso *et al.*, "Whitlockite has a characteristic distribution in mammary microcalcifications and it is not associated with breast cancer," *Cancer Communications*, vol. 43, no. 10, pp. 1169–1173, 2023. doi: *https://doi.org/10.1002/cac2.12481*.

[9] L. B. Resnikoff, E. B. Mendelson, C. E. Tobin, and T. M. Hendrix, "Breast imaging case of the day. Metastatic calcification in the breast from secondary hyperparathyroidism induced by chronic renal failure," *RadioGraphics*, vol. 16, no. 6, pp. 1512–1513, 1996. doi: *10.1148/radiographics.16.6.8946553*.

[10] G. Pettinato, C. J. Manivel, L. Panico, L. Sparano, and G. Petrella, "Invasive Micropapillary Carcinoma of the Breast: Clinicopathologic Study of 62 Cases of a Poorly Recognized Variant With Highly Aggressive Behavior," *American Journal of Clinical Pathology*, vol. 121, no. 6, pp. 857–866, Jan. 2004, doi: *10.1309/XTJ7VHB49UD78X60*.

[11] B. Mujtaba *et al.*, "Heterotopic ossification: radiological and pathological review," *Radiology and Oncology*, vol. 53, no. 3, pp. 275–284, 2019. doi: *10.2478/raon-2019-0039*.

[12] D. Hackel et al., "Enabling Microsegmentation: Digital Pathology Corpora for Advanced Model Development," in *Signal Processing in Medicine and Biology: Applications of Artificial Intelligence in Medicine and Biology*, vol. 1, New York City, New York, USA: Springer, 2026, p. 50. [Online]. Available: *https://isip.piconepress.com/publications/book_sections/2026/springer/dpath/* (in publication).

[13] S. S. Shalamzari *et al.*, "Big Data Resources for Digital Pathology," in *Proceedings of the IEEE Signal Processing in Medicine and Biology Symposium*, Philadelphia, Pennsylvania, USA: IEEE, 2023, pp. 1–19. doi: *10.1109/SPMB59478.2023.10372721.*.

[14] G. Lemaître, F. Nogueira, and C. K. Aridas, "Imbalanced-learn: A Python Toolbox to Tackle the Curse of Imbalanced Datasets in Machine Learning," *Journal of Machine Learning Research*, vol. 18, no. 17, pp. 1–5, 2017. url: *dl.acm.org/doi/pdf/10.5555/3122009.3122026*.

[15] B. Doshna, Z. Wevodau, N. Jhala, I. Akhtar, I. Obeid, and J. Picone, "The Temple University Digital Pathology Corpus: The Breast Tissue Subset," in *Proceedings of the IEEE Signal Processing in Medicine and Biology Symposium (SPMB)*, I. Obeid, I. Selesnick, and J. Picone, Eds., Philadelphia, Pennsylvania, USA: IEEE, 2021, pp. 1–3. doi: 10.1109/SPMB52430.2021.9672275.